Two-photon excitation to autoionizing states of He detected via radiative cascades to the metastable states

Andrej Mihelič[1,*] and Matjaž Žitnik[1,2]

[1]*Jožef Stefan Institute, Jamova cesta 39, SI-1000 Ljubljana, Slovenia*

[2]*Faculty of mathematics and physics, University of Ljubljana, Jadranska cesta 19, SI-1000 Ljubljana, Slovenia*

(Received 9 April 2015; published 15 June 2015)

We present a detailed theoretical study of two-photon above-threshold excitation to the lowest dipole forbidden $^1S^e$ and $^1D^e$ autoionizing states of helium with free-electron-laser pulses. We consider the case where the formation of these transient states is detected by monitoring the yield of atoms in the metastable $1s2s$ states, which are reached in the radiative cascade decays of the autoionizing states. We describe the two-photon near-resonant driving with an effective Hamiltonian operator within the density matrix formalism, and we report the relevant parameters of the model, such as the field-induced shifts, the effective Rabi frequencies, and the cascade branching ratios of both the autoionizing states and the $1sn\ell$ states, to which the autoionizing states decay. We compare the calculated metastable atom yield to the vacuum ultraviolet florescence yield and to the electron yield. We discuss the effects of the intensity of the source, admixture of higher harmonics in the incident beam, polarization of the incident light, and the pulse chirp on the metastable atom yield.

DOI: 10.1103/PhysRevA.91.063409 PACS number(s): 32.80.Rm, 41.60.Cr, 31.15.ac, 32.80.Zb

I. INTRODUCTION

Over the past decades, advances in the development of free-electron-laser (FEL) sources have led to the generation of intense, short-wavelength radiation ranging from extreme ultraviolet to x rays, with pulse duration of the order of (few tens of) femtoseconds [1–3]. While the sources based on self-amplified spontaneous emission (SASE) [1–4], which are characterized by lower shot-to-shot spectral and temporal stability, can be used to perform spectral analysis using appropriately sorted single-shot FEL spectra (e.g., see Ref. [5]), a more convenient scheme for producing stable FEL pulses is the one based on generation at the harmonics of an external seed laser [high-gain harmonic generation (HGHG)] [6–9]. The HGHG sources are especially important when scans are required over energy regions narrower or comparable to the range of energy fluctuations exhibited by the source.

Very recently, an experiment was performed by Žitnik *et al.* [10] in which the lowest dipole forbidden $^1S^e$ and $^1D^e$ autoionizing states of the helium atom were studied by two-photon absorption using intense femtosecond pulses generated by the seeded FEL source FERMI at Elettra. The experiment was performed at the Low density matter end station [11] and exploited the scanning capabilities of the source [9]. The autoionizing states studied in Ref. [10] lie in the energy region between 59.5 and 64.5 eV above the ground state; thus the energies of the incident photons were of the order of 30 eV (wavelengths ∼40 nm), i.e., above the ionization threshold of helium. Identification of the two-photon process poses a challenge in this case since the dominant mechanism, single-photon ionization, is responsible for a large background signal in the measured electron and ion yields. This is why excitation to the autoionizing states was studied by monitoring the yield of neutral atoms in the metastable singlet and triplet $1s2s$ states, to which the autoionizing states cascade with low probability when they decay radiatively. Unlike the ion or electron yield, the metastable atom yield is background free. Its increase is unambiguously associated with excitation to a resonance state, as described in the following.

Autoionizing states of helium represent a subset of doubly excited states (DES), often said to be the prototypical atomic states for studying electron correlations. Since the experiment performed by Madden and Codling [12], these states have been extensively studied both experimentally and theoretically (see Ref. [13] for a review). Apart from the studies dealing with the properties of dipole forbidden DES through interaction with dipole allowed DES in external electric [14–17] and magnetic fields [18] or through dipole-quadrupole interference [19,20], the dipole allowed DES have, to date, mostly been studied experimentally. While autoionization is usually the most probable decay mechanism of the DES, it became clear that their radiative decay is important for a detailed interpretation of photoabsorption spectra [21–23]. A relatively simple alternative detection scheme, which can be used to observe the radiative decay of DES indirectly, was shown to be the aforementioned detection of atoms in the $1s2s$ states [24]. This scheme was used to detect the previously unobserved triplet DES [25,26]. Although the decay branching ratios of the DES to cascade to the $1s2s$ states are relatively low, the metastable atom yield detection is efficient as it does not depend on the detector acceptance angle (in contrast with the fluorescence yield): excited helium atoms are detected in a head-on collision of the collimated beam with the metastable atom detector.

In this work we present a theory which is used for the description of two-photon above-threshold excitation to the $^1S^e$ and $^1D^e$ autoionizing states with intense femtosecond FEL pulses. The in-depth theoretical study we present here was used as a basis for the experiment described in Ref. [10]: it served as the feasibility study and for the interpretation of the experimental results.

II. FORMULATION

We consider ground-state helium atoms irradiated by FEL pulses of peak intensity $\sim 10^{14}$ W/cm^2 and pulse duration

*andrej.mihelic@ijs.si

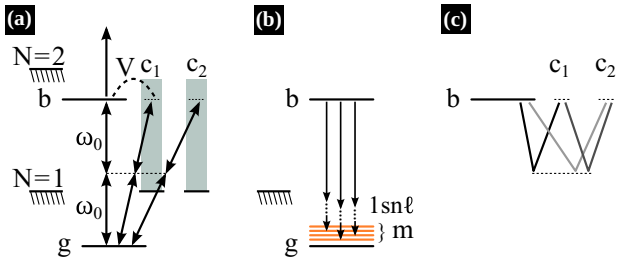

FIG. 1. (Color online) (a) Two-photon above-threshold excitation of the ground-state (g) atom to the discrete state (b) embedded in the continuum (c_1). The arrows represent absorption and emission of photons with energy ω_0, and V (dashed line) denotes configuration interaction (CI). The continuum not coupled to the discrete state via CI is labeled by c_2. (b) Cascade decay of the autoionizing state to the $1s2s$ metastable states (m). (c) The paths neglected in the present treatment.

of the order of 100 fs. Let $|g\rangle$ be the atomic ground state and $|b\rangle$ the discrete state embedded in the continuum, which we denote by $|c_1\rangle$. Furthermore, let $|c_2\rangle$ be the continuum which is unreachable from $|b\rangle$ by autoionization [Fig. 1(a)]. The discrete state and the two continua are accessible from the ground state by two-photon absorption. We denote the energies corresponding to $|g\rangle$, $|b\rangle$, $|c_1\rangle$, and $|c_2\rangle$ by ϵ_g, ϵ_b, ϵ_{c_1}, and ϵ_{c_2}. The energy of the incident photons (ω_0) lies above the first ($N = 1$) ionization threshold (24.59 eV above the ground state), so that the excitation proceeds through the $^1P^o$ continuum ($1s\epsilon p$). It is assumed that two-photon excitation is near-resonant, i.e., $\epsilon_b \approx \epsilon_g + 2\omega_0$, and that no intermediate resonance state lies close to $\epsilon_g + \omega_0$. Since the excitation proceeds from the helium ground state, the symmetry of $|b\rangle$ and $|c_1\rangle$ is $^1S^e$ and the symmetry of $|c_2\rangle$ is $^1D^e$ or vice versa. The atom in the autoionizing (resonance) state may be further ionized by the laser. Alternatively, state $|b\rangle$ can decay by photon emission [Fig. 1(b)]. The resonance states below the $N = 2$ threshold, which are of interest here, decay radiatively almost exclusively to the $1sn\ell$ states. These states, in turn, cascade either to the ground state or to the metastable (MS) singlet and triplet $1s2s$ states [denoted by m in Fig. 1(b)]. Note that the direct (noncascade) decay of state $|b\rangle$ to the MS states is dipole forbidden. The lifetimes of the singlet and triplet $1s2s$ states are long (20 ms and 8000 ms, respectively [27,28]) compared to the time of flight of the atoms to the metastable atom detector, so that these states may be treated as stable.

The decay widths of the resonance states we consider are taken to be small compared to their energy differences, so that the states do not overlap. We assume that the intensity is low enough and the pulse duration long in comparison with the period of the field ($2\pi/\omega_0$), so that the driving by the laser is describable in terms of the second-order transition amplitudes. Furthermore, we assume that the continuum-continuum coupling, i.e., the coupling between the $1s\epsilon p$ continuum and $|c_1\rangle$ and $|c_2\rangle$ ($1s\epsilon s$ and $1s\epsilon d$), is weak. The effect of the laser on the states is taken into account through laser-induced decay widths and energy shifts [29–31]. Here we employ the density matrix formalism in which the radiation field is treated classically. The effective Hamiltonian operator which describes the atom interacting with the laser field in the rotating wave approximation is written as [29–33]

$$H = H_0 + V + \bar{D}, \tag{1a}$$

$$\begin{aligned} H_0 = {} & (\epsilon_g + S_g - i\gamma_g/2)|g\rangle\langle g| \\ & + \left(\epsilon_b + S_b - i\gamma_b/2 - i\Gamma_b^f/2\right)|b\rangle\langle b| \\ & + \int d\epsilon_{c_1}\epsilon_{c_1}|c_1\rangle\langle c_1| + \int d\epsilon_{c_2}\epsilon_{c_2}|c_2\rangle\langle c_2|, \end{aligned} \tag{1b}$$

$$V = \int d\epsilon_{c_1} V_{bc_1}|b\rangle\langle c_1| + \int d\epsilon_{c_1} V_{c_1 b}|c_1\rangle\langle b|, \tag{1c}$$

$$\bar{D} = \sum\!\!\!\!\!\!\int_j \frac{\bar{\Omega}_{jg}}{2} e^{-2i\omega_0 t}|j\rangle\langle g| + \sum\!\!\!\!\!\!\int_j \frac{\bar{\Omega}_{gj}}{2} e^{2i\omega_0 t}|g\rangle\langle j|, \tag{1d}$$

where V is the configuration-interaction (CI) operator and $\bar{D}$ the effective two-photon transition operator. In the present formalism, states $|g\rangle$, $|b\rangle$, $|c_1\rangle$, and $|c_2\rangle$ are the eigenstates of operator H_0 with complex eigenenergies which include the field-induced shifts (S_g and S_b) and the field-induced decay widths (γ_g and γ_b) defined in the following. In addition, decay width Γ_b^f has been included to account for the spontaneous (fluorescence) decay of state $|b\rangle$. The sums with the integral sign in Eq. (1d) include the integration over the energies of the continua, and j runs over b, c_1, and c_2. The two-photon Rabi frequencies are

$$\bar{\Omega}_{jg} = \frac{\mathcal{F}^2}{2} \sum\!\!\!\!\!\!\int_\nu \frac{D_{j\nu} D_{\nu g}}{\epsilon_g + \omega_0 - \epsilon_\nu + i\eta}, \tag{2a}$$

$$\bar{\Omega}_{gj} = \frac{\mathcal{F}^2}{2} \sum\!\!\!\!\!\!\int_\nu \frac{D^\dagger_{g\nu} D^\dagger_{\nu j}}{\epsilon_g + \omega_0 - \epsilon_\nu + i\eta}, \tag{2b}$$

where ν runs over the bound and continuum intermediate $^1P^o$ states, $\mathcal{F} = \mathcal{F}(t)$ is the envelope of the electric field of the laser pulse (assumed real), and the limit $\eta \to 0^+$ is implied. The electric dipole operator is $D = \hat{\boldsymbol{e}}_0 \cdot (\boldsymbol{r}_1 + \boldsymbol{r}_2)$, where $\hat{\boldsymbol{e}}_0$ is the unit polarization vector, and $\boldsymbol{r}_1$ and $\boldsymbol{r}_2$ are the electron coordinates. Laser-induced shifts S_g and S_b and laser-induced widths γ_g and γ_b of states $|g\rangle$ and $|b\rangle$ are defined by [29]

$$S_g - i\gamma_g/2 = \frac{\mathcal{F}^2}{4} \sum\!\!\!\!\!\!\int_\nu \frac{|D_{\nu g}|^2}{\epsilon_g + \omega_0 - \epsilon_\nu + i\eta}, \tag{3a}$$

$$\begin{aligned} S_b - i\gamma_b/2 = {} & \frac{\mathcal{F}^2}{4} \sum\!\!\!\!\!\!\int_\mu \left\{ \frac{|D_{\mu b}|^2}{\epsilon_b + \omega_0 - \epsilon_\mu + i\eta} \right. \\ & \left. + \frac{|D_{\mu b}|^2}{\epsilon_b - \omega_0 - \epsilon_\mu + i\eta} \right\}. \end{aligned} \tag{3b}$$

The generalized sums in Eq. (3a) and Eq. (3b) run over the $^1P^o$ and over the $^1P^o$ and $^1F^o$ bound and continuum states, respectively. The terms which correspond to both positive and negative frequencies (i.e., describe absorption and stimulated emission) are required in Eq. (3b) for the calculation of S_b (see Sec. III B). In the present formalism, the decay widths of

the bound intermediate states have been neglected because of the large detunings ($\omega_0 - \epsilon_\nu + \epsilon_g$), and only the continuum intermediate states therefore contribute to γ_g and γ_b. The latter thus describe single-photon ionization of the atom in the ground state and in the resonance state, respectively. The integrals in Eqs. (3a) and (3b) are evaluated by taking into account that the (dipole) matrix elements vary slowly with the energy and by using the relation $\lim_{\eta\to 0^+}(x+i\eta)^{-1} = \mathcal{P}x^{-1} - i\pi\delta(x)$, where $\mathcal{P}$ denotes the Cauchy principal value.

Our initial assumption has been that the driving be describable in terms of the second-order transition amplitudes. In this approximation, we have neglected the indirect coupling by the laser between $|b\rangle$, $|c_1\rangle$, and $|c_2\rangle$ via stimulated emission and subsequent absorption of photons, as has been depicted in Fig. 1(c). This approximation is valid when the intensity is low enough, i.e., when

$$\frac{\mathcal{F}^2}{4}\left|\sum\!\!\!\!\!\!\int_\nu \frac{\langle k|D|\nu\rangle\langle\nu|D^\dagger|j\rangle}{\epsilon_g+\omega_0-\epsilon_\nu+i\eta}\right| \ll \left|V_{c_1 b}\right| \tag{4}$$

holds for $j,k \in \{b,c_1,c_2\}$. Note that this is consistent with the assumption that the continuum-continuum coupling (described by $\langle c_1|D|\nu\rangle$ and $\langle c_2|D|\nu\rangle$ when $|\nu\rangle$ is a continuum state) is weak. The reader is referred to Ref. [34] for a discussion.

We write the solution of the Schrödinger equation in terms of the slowly varying amplitudes, a_g, a_b, a_{c_1}, and a_{c_2}:

$$\begin{aligned}|\Psi(t)\rangle = {}& a_g(t)e^{-i(\epsilon_g+S_g)t}|g\rangle + a_b(t)e^{-i(\epsilon_g+S_g+2\omega_0)t}|b\rangle \\ &+ \int d\epsilon_{c_1} a_{c_1}(t)e^{-i(\epsilon_g+S_g+2\omega_0)t}|c_1\rangle \\ &+ \int d\epsilon_{c_2} a_{c_2}(t)e^{-i(\epsilon_g+S_g+2\omega_0)t}|c_2\rangle.\end{aligned} \tag{5}$$

This leads to the following system of coupled differential equations:

$$\begin{aligned} i\frac{d}{dt}a_g =& -i\frac{\gamma_g}{2}a_g + \frac{\bar\Omega_{gb}}{2}a_b + \int d\epsilon_{c_1}\frac{\bar\Omega_{gc_1}}{2}a_{c_1} \\ &+ \int d\epsilon_{c_2}\frac{\bar\Omega_{gc_2}}{2}a_{c_2}, \end{aligned} \tag{6a}$$

$$\begin{aligned} i\frac{d}{dt}a_b =& \left(-\Delta_b - i\frac{\gamma_b}{2} - i\frac{\Gamma_b^f}{2}\right)a_b + \frac{\bar\Omega_{bg}}{2}a_g \\ &+ \int d\epsilon_{c_1} V_{bc_1}a_{c_1}, \end{aligned} \tag{6b}$$

$$i\frac{d}{dt}a_{c_1} = -\Delta_{c_1}a_{c_1} + \frac{\bar\Omega_{c_1 g}}{2}a_g + V_{c_1 b}a_b, \tag{6c}$$

$$i\frac{d}{dt}a_{c_2} = -\Delta_{c_2}a_{c_2} + \frac{\bar\Omega_{c_2 g}}{2}a_g, \tag{6d}$$

where we have introduced detunings $\Delta_b = 2\omega_0 - (\epsilon_b + S_b) + \epsilon_g + S_g$, $\Delta_{c_1} = 2\omega_0 - \epsilon_{c_1} + \epsilon_g + S_g$, and $\Delta_{c_2} = 2\omega_0 - \epsilon_{c_2} + \epsilon_g + S_g$. We proceed by integrating Eqs. (6c) and (6d) and inserting the expressions into Eqs. (6a) and (6b). Next, we take into account that the Rabi frequencies $\bar\Omega_{c_1 g}$, $\bar\Omega_{c_2 g}$, $\bar\Omega_{gc_1}$, and $\bar\Omega_{gc_2}$ and the CI matrix elements vary slowly with ϵ_{c_1} and ϵ_{c_2}, so that the Markov approximation [35,36] may be used. Applying the Markov approximation is equivalent to ignoring the derivatives in Eqs. (6c) and (6d) [32,37]:

$$a_{c_1} \approx \frac{\bar\Omega_{c_1 g}a_g/2 + V_{c_1 b}a_b}{\Delta_{c_1} + i\eta}, \tag{7a}$$

$$a_{c_2} \approx \frac{\bar\Omega_{c_2 g}a_g/2}{\Delta_{c_2} + i\eta}, \tag{7b}$$

and leads to the following equations:

$$\frac{d}{dt}a_g = -\frac{\bar\Gamma_g}{2}a_g - i\frac{\tilde\Omega_{gb}}{2}\left(1 - \frac{i}{q_{gb}}\right)a_b, \tag{8a}$$

$$\frac{d}{dt}a_b = \left(i\bar\Delta_b - \frac{\bar\Gamma_b}{2}\right)a_b - i\frac{\tilde\Omega_{bg}}{2}\left(1 - \frac{i}{q_{bg}}\right)a_g. \tag{8b}$$

We have defined the detuning as

$$\bar\Delta_b = 2\omega_0 - (\epsilon_b + S_b + F_b) + \epsilon_g + S_g + \bar S_g, \tag{9}$$

the total decay width of the ground state as $\bar\Gamma_g = \gamma_g + \bar\gamma_g$, and the total decay width of the resonance state as $\bar\Gamma_b = \Gamma_b^a + \Gamma_b^f + \gamma_b$. The autoionization width Γ_b^a and the shift F_b due to the CI are obtained from

$$F_b - i\Gamma_b^a/2 = \mathcal{P}\int d\epsilon_{c_1}\frac{\left|V_{c_1 b}\right|^2}{\Delta_{c_1}} - i\pi\left|V_{c_1 b}\right|^2. \tag{10}$$

The energy shift and energy width due to two-photon absorption and emission are

$$\bar S_g - i\frac{\bar\gamma_g}{2} = \frac{1}{4}\int d\epsilon_{c_1}\frac{\bar\Omega_{gc_1}\bar\Omega_{c_1 g}}{\Delta_{c_1}+i\eta} + \frac{1}{4}\int d\epsilon_{c_2}\frac{\bar\Omega_{gc_2}\bar\Omega_{c_2 g}}{\Delta_{c_2}+i\eta}, \tag{11}$$

The two-photon Rabi frequencies used in Eqs. (8a) and (8b) are

$$\tilde\Omega_{bg} = \frac{\mathcal{F}^2}{2}\sum\!\!\!\!\!\!\int_\nu \frac{\langle\tilde b|D|\nu\rangle\langle\nu|D|g\rangle}{\epsilon_g+\omega_0-\epsilon_\nu+i\eta}, \tag{12a}$$

$$\tilde\Omega_{gb} = \frac{\mathcal{F}^2}{2}\sum\!\!\!\!\!\!\int_\nu \frac{\langle g|D^\dagger|\nu\rangle\langle\nu|D^\dagger|\tilde b\rangle}{\epsilon_g+\omega_0-\epsilon_\nu+i\eta}, \tag{12b}$$

and describe the coupling by the laser between the ground state and the discrete state modified by the admixture of the continuum:

$$|\tilde b\rangle = |b\rangle + \mathcal{P}\int d\epsilon_{c_1}\frac{|c_1\rangle V_{c_1 b}}{\Delta_{c_1}}. \tag{13}$$

The asymmetry (Fano) parameters [38] associated with two-photon transitions between the ground state and the resonance state are

$$q_{bg} = \frac{\tilde\Omega_{bg}}{\pi V_{bc_1}\bar\Omega_{c_1 g}}, \tag{14a}$$

$$q_{gb} = \frac{\tilde\Omega_{gb}}{\pi \bar\Omega_{gc_1} V_{c_1 b}}, \tag{14b}$$

and are independent of the intensity of the laser under the approximations used here. It should be noted that $\tilde\Omega_{bg}$ and

$\tilde{\Omega}_{gb}$, as well as q_{gb} and q_{bg}, are complex since the excitation proceeds through the continuum [39,40]. The expressions for the asymmetry parameters agree with the ones given in Ref. [40] for a single open continuum channel and an isolated resonance state. Since the polarization-dependent factors can be factored out of the numerators and denominators in Eqs. (14a) and (14b), it can be shown that q_{bg} and q_{gb} are independent of $\hat{\boldsymbol{e}}_0$. Consequently, $q_{bg} = q_{gb}$ may be shown to hold.

Using Eqs. (8a) and (8b), the following density matrix equations can be derived:

$$\frac{d}{dt}\rho_{gg} = -\bar{\Gamma}_g\rho_{gg} + \mathrm{Im}\left\{\tilde{\Omega}_{gb}\left(1 - \frac{i}{q_{gb}}\right)\rho_{bg}\right\}, \tag{15a}$$

$$\frac{d}{dt}\rho_{bb} = -\bar{\Gamma}_b\rho_{bb} + \mathrm{Im}\left\{\tilde{\Omega}_{bg}\left(1 - \frac{i}{q_{bg}}\right)\rho^*_{bg}\right\}, \tag{15b}$$

$$\frac{d}{dt}\rho_{bg} = \left(i\bar{\Delta}_b - \frac{\bar{\Gamma}_g}{2} - \frac{\bar{\Gamma}_b}{2} - \gamma_L\right)\rho_{bg} - i\frac{\tilde{\Omega}_{bg}}{2}\left(1 - \frac{i}{q_{bg}}\right)\rho_{gg} + i\frac{\tilde{\Omega}^*_{gb}}{2}\left(1 + \frac{i}{q^*_{gb}}\right)\rho_{bb}, \tag{15c}$$

where $\rho_{jk} = a_j a^*_k$. An additional decay term $(-\gamma_L\rho_{bg})$ has been included on the right-hand side of Eq. (15c), where γ_L is a transverse relaxation rate used to describe, for example, phase fluctuations of the driving field [41]. Equations similar to (15a)–(15c) have been obtained in Refs. [31–33]. Note, however, that unlike the asymmetry parameters used in Refs. [30–33], q_{gb} and q_{bg} are complex, as already mentioned.

The fluorescence yield (y_f) and the yield of atoms in the MS states (y_m), to which the resonance state cascades, can be calculated in a straightforward way from

$$\frac{d}{dt}y_f = \Gamma^f_b\rho_{bb}, \tag{16a}$$

$$\frac{d}{dt}y_m = \Gamma^m_b\rho_{bb}. \tag{16b}$$

Here, Γ^m_b denotes the cascade decay rate of state $|b\rangle$ to the MS states (see Sec. III B). The electron yield due to two-photon absorption (y_e) is calculated as follows. From Eqs. (6c) and (6d) we obtain equations of motion for the diagonal matrix elements:

$$\frac{d}{dt}\rho_{c_1c_1} = -\mathrm{Im}\left\{\bar{\Omega}^*_{c_1g}\rho_{c_1g} + 2V^*_{c_1b}\rho_{c_1b}\right\}, \tag{17a}$$

$$\frac{d}{dt}\rho_{c_2c_2} = -\mathrm{Im}\left\{\bar{\Omega}^*_{c_2g}\rho_{c_2g}\right\}. \tag{17b}$$

We integrate Eqs. (17a) and (17b) over ϵ_{c_1} and ϵ_{c_2}, where we take into account again that $\bar{\Omega}_{c_1g}$, $\bar{\Omega}_{c_2g}$, and V_{c_1b} vary slowly with ϵ_{c_1} and ϵ_{c_2}. By using Eqs. (7a) and (7b) to eliminate ρ_{c_1g}, ρ_{c_1b}, and ρ_{c_2g}, the total ionization rate is seen to be equal to

$$\frac{d}{dt}y_e = \int d\epsilon_{c_1}\left(d\rho_{c_1c_1}/dt\right) + \int d\epsilon_{c_2}\left(d\rho_{c_2c_2}/dt\right) \tag{18a}$$

$$= \Re_g\rho_{gg} + \Gamma^a_b\rho_{bb} + 2\,\mathrm{Re}\,\frac{\tilde{\Omega}_{bg}\rho^*_{bg}}{q_{bg}}, \tag{18b}$$

where $\Re_g = \pi\left|\bar{\Omega}_{c_1g}\right|^2/2 + \pi\left|\bar{\Omega}_{c_2g}\right|^2/2$ the first two terms in Eq. (18b) describe the background two-photon ground-state photoionization and autoionization of $|b\rangle$, respectively. The last term in Eq. (18b) arises due to the coupling (CI) between $|b\rangle$ and $|c_1\rangle$, i.e., due to the "interference" between the direct pathway to the continuum and the indirect pathway through the discrete state. Note that the ionization rate can also be calculated directly from

$$\frac{dy_e}{dt} = 2\pi\{|\langle c_1|V + \bar{D}|\Psi(t)\rangle|^2 + |\langle c_2|\bar{D}|\Psi(t)\rangle|^2\} \tag{19a}$$

$$= 2\pi\left\{\left|\bar{\Omega}_{c_1g}a_g/2 + V_{c_1b}a_b\right|^2 + \left|\bar{\Omega}_{c_2g}a_g/2\right|^2\right\}, \tag{19b}$$

where the first and the second term in Eqs. (19a) and (19b) describe the transitions to the two continua.

As the incident photon energies lie in the energy region between the $N = 1$ and $N = 2$ ionization threshold, photoionization (autoionization) results in ions in the ground state. Since the latter does not decay radiatively, both the fluorescence and the MS atom yield are background-free, i.e., the single-photon process does not contribute to the background signal. This does not hold for the electron yield: photoelectron kinetic-energy analysis is required to differentiate between electrons ejected in the one- and two-photon process.

We may obtain an approximate solution of the Schrödinger equation for the whole energy region of the resonance states in the following way. Since the resonances considered are nonoverlapping, we may simply sum over the resonance states (b) on the right-hand sides of Eqs. (15a), (16a), (16b), and (18b). For $I_0 \lesssim 10^{15}$ W/cm^2, the yields thus calculated are practically indistinguishable from the yields obtained in the calculation in which the full system of coupled differential equations describing the density matrix is solved.

III. CALCULATIONS

The bound and continuum atomic states have been represented in a basis of real two-electron Coulomb-Sturmian wave functions [42,43]. The method of complex scaling [44] has been used to calculate the parameters associated with the resonance states.

While the singlet-triplet coupling among the resonance states is weak [45] and has been neglected, it has been found to be essential for the $1s n\ell$ states. The mixing among the ^1L_L and ^3L_L $1snL$ states is strong for total orbital angular momentum $L \geqslant 3$ [46]. When the cascade proceeds through these states, the probability to reach the MS states is increased: the $1s n\ell$ states for which the singlet-triplet coupling is strong are more likely to cascade to the triplet $1s2s$ states. In particular, the $^1D^e$ resonances decay directly to the $1snf$ states, which cascade to the MS states with higher probability than the $1snp$

states with predominantly singlet character (these are most likely populated in the decay of the $^1S^e$ and $^1D^e$ resonance states).

A. Branching ratios of the $1s n\ell$ states

The decay widths of the singlet-triplet mixed $1sn\ell$ states have been obtained by combining the dipole matrix elements of the calculated LSJ-coupled wave functions with the values of the singlet-triplet mixing coefficients and accurate energies (these include relativistic and QED corrections) from the high precision calculations (see Refs. [46–48]).

If β_h^s and β_k^s denote the coefficients of the singlet LSJ-coupled basis states $|h_s\rangle$ and $|k_s\rangle$ and β_h^t and β_k^t the analogous coefficients of the triplet basis states $|h_t\rangle$ and $|k_t\rangle$, the singlet-triplet mixed states $|h\rangle$ and $|k\rangle$ are written as

$$|h\rangle = \beta_h^s|h_s\rangle + \beta_h^t|h_t\rangle, \tag{20a}$$

$$|k\rangle = \beta_k^s|k_s\rangle + \beta_k^t|k_t\rangle. \tag{20b}$$

The $|k\rangle \to |h\rangle$ partial decay width and the total decay width are then calculated as

$$\Gamma_{h,k} = \frac{4\alpha^3}{3}(\epsilon_k - \epsilon_h)^3 \begin{pmatrix} J_h & 1 & J_k \\ -M_h & M_h - M_k & M_k \end{pmatrix}^2 \times \langle h\|D\|k\rangle^2, \tag{21a}$$

$$\Gamma_k = \sum_h \Gamma_{h,k}, \tag{21b}$$

where α denotes the fine-structure constant, J_h and J_k are the total angular momenta of states $|h\rangle$ and $|k\rangle$, M_h and M_k the corresponding projections, and $\langle h\|D\|k\rangle = \beta_h^s\beta_k^s\langle h_s\|D\|k_s\rangle + \beta_h^t\beta_k^t\langle h_t\|D\|k_t\rangle$ denotes the reduced dipole matrix element.

The branching ratio of state $|k\rangle$ to cascade to the MS states is [48]

$$\mathcal{B}_k^m = \sum_j \left\{ \frac{\Gamma_{j,k}}{\Gamma_k} + \sum_{\mathfrak{n}=2}^{\infty} \sum_{h_2,\ldots,h_\mathfrak{n}} \frac{\Gamma_{j,h_\mathfrak{n}}}{\Gamma_{h_\mathfrak{n}}} \cdots \frac{\Gamma_{h_3,h_2}}{\Gamma_{h_2}} \frac{\Gamma_{h_2,k}}{\Gamma_k} \right\}, \tag{22}$$

where j runs over the singlet and triplet $1s2s$ states. The first term in Eq. (22) describes the direct transition from $|k\rangle$ to $|j\rangle$ and the second term the $\mathfrak{n}$-step cascade transition which proceeds through states $|h_2\rangle, \ldots, |h_\mathfrak{n}\rangle$. The effective decay rate is calculated as $\Gamma_k^m = \mathcal{B}_k^m\Gamma_k$.

The branching ratios of the $1snp$ and $1snf$ states with a nonzero singlet basis state admixture can be found in Table I. As mentioned, the branching ratios of the states with $L \geqslant 3$ are high due to the strong singlet-triplet mixing, resulting in an increased probability to cascade to the triplet $1s2s$ states. Decay branching ratios of the $1sn\ell$ states calculated in a similar way as in Eq. (22) were recently used to reproduce the dependence of the MS atom yield on the strength of a tunable static electric field with high accuracy [48]: the positions and shapes of the structures in the measured yield, which were the consequence of the strong field-induced mixing, were shown to be in very good agreement with the results of the calculations.

B. Resonance parameters

We have used the method of complex scaling [43,44] to calculate the parameters of the resonance states. In this formalism, each resonance state is associated with a single eigenvector $|b_\theta\rangle$ of the complex-scaled Hamiltonian operator $H(\theta)$, where θ denotes the rotation angle. The corresponding eigenvalues can be written as $E_b^\theta = \tilde{\epsilon}_b - i\Gamma_b^a/2$, where Γ_b^a is the autoionization decay width and $\tilde{\epsilon}_b$ is the energy of the resonance state which already includes F_b [Eq. (10)].

The generalized Rabi frequencies have been calculated using the following relations:

$$\tilde{\Omega}_{bg}\left(1 - \frac{i}{q_{bg}}\right) = \frac{\mathcal{F}^2}{2}\sum_\nu \frac{\langle b_\theta^*|D_\theta|\nu_\theta\rangle\langle\nu_\theta^*|D_\theta|g_\theta\rangle}{\epsilon_g + \omega_0 - E_\nu^\theta}, \tag{23a}$$

$$\tilde{\Omega}_{gb}\left(1 - \frac{i}{q_{gb}}\right) = \frac{\mathcal{F}^2}{2}\sum_\nu \frac{\langle g_\theta^*|D_\theta^\dagger|\nu_\theta\rangle\langle\nu_\theta^*|D_\theta^\dagger|b_\theta\rangle}{\epsilon_g + \omega_0 - E_\nu^\theta}, \tag{23b}$$

where $|\nu_\theta\rangle$ and E_ν^θ denote the eigenstates and the eigenenergies of $H(\theta)$ of $^1P^o$ symmetry, $D_\theta = e^{i\theta}D$, and $D_\theta^\dagger = e^{i\theta}D^\dagger$. The complex-scaled ground state is denoted by $|g_\theta\rangle$. The conjugation sign in $\langle b_\theta^*|$, $\langle\nu_\theta^*|$, and $\langle g_\theta^*|$ means that the deconjugated radial parts of the wave functions should be used in the calculation of the matrix elements. It is important to note that the two-photon transition amplitudes calculated by means of the complex-scaled states—described by the right-hand sides of Eqs. (23a) and (23b)—are associated with $\tilde{\Omega}_{bg}(1 - i/q_{bg})$ and $\tilde{\Omega}_{gb}(1 - i/q_{gb})$. This was discussed in Ref. [37] for the case of the single-photon coupling. The discussion used there also remains valid in the present case if the dipole operators, D and $D^\dagger$, are replaced with two-photon transition operators $DG^+(\epsilon_g + \omega_0)D$ and $D^\dagger G^+(\epsilon_g + \omega_0)D^\dagger$, where $G^+(\epsilon) = (\epsilon + i\eta - H_0 - V)^{-1}$ denotes the retarded Green's operator.

As has been mentioned, the singlet-triplet mixing among the resonance states has been neglected. In this approximation, only the resonances of the $^1S^e$ and $^1D^e$ symmetry are accessible. These resonances decay to those $1snp$ and $1snf$ states $\{|k\rangle\}$ that have a nonzero admixture of the singlet basis state ($\beta_k^s \neq 0$). Furthermore, the direct decay of the resonance state to the MS states is dipole forbidden. Decay rate Γ_b^m of the resonance state may therefore be assessed from the cascade branching ratio of state $|b\rangle$:

$$\mathcal{B}_b^m = \sum_k \mathcal{B}_k^m \frac{\Gamma_{k,b}^f}{\Gamma_b^f + \Gamma_b^a} \equiv \frac{\Gamma_b^m}{\Gamma_b^f + \Gamma_b^a}, \tag{24}$$

where $\mathcal{B}_k^m$ is the branching ratio of state $|k\rangle$ (Sec. III A) and $\Gamma_{k,b}^f$ is the $|b\rangle \to |k\rangle$ partial decay width (cf. Refs. [43,49]):

$$\Gamma_{k,b}^f \approx \frac{4\alpha^3}{3}(\epsilon_b - \epsilon_k)^3 \begin{pmatrix} J_k & 1 & J_b \\ -M_k & M_k - M_b & M_b \end{pmatrix}^2 \times \left|\beta_k^s\right|^2 \mathrm{Re}\{\langle k_{s,\theta}^*\|D_\theta\|b_\theta\rangle^2\}. \tag{25}$$

The total angular momentum of the resonance state and state $|k\rangle$ and their projections are denoted by J_b, J_k, M_b, and M_k. The complex scaled state which corresponds to the singlet basis state ($|k_s\rangle$) has been denoted by $|k_{s,\theta}\rangle$. Only the $1snp$ and $1snf$ final states have been considered in Eq. (24) since the partial decay rates of $|b\rangle$ to the lower-lying DES have been found to be much smaller. Equation (25) gives the (partial) decay width of the discrete part of the autoionizing state

TABLE I. Decay branching ratios $\mathcal{B}_k^m$ and decay widths Γ_k of the $1snℓ$ states. Only the ratios of the states with nonzero singlet component β_k^s are shown. The numbers in parentheses denote the powers of ten.

$n\,L_J$	$-\epsilon_k$	$\lvert\beta_k^s\rvert^2$	Γ_k	$\mathcal{B}_k^m$	$n\,L_J$	$-\epsilon_k$	$\lvert\beta_k^s\rvert^2$	Γ_k	$\mathcal{B}_k^m$
$2\,P_1$	2.1238389034	1.0000	4.355(−8)	1.097(−3)	$8\,P_1$	2.0079471379	5.9878(−8)	3.383(−11)	9.998(−1)
$2\,P_1$	2.1331718034	7.7451(−8)	2.470(−10)	1.000	$8\,D_2$	2.0078165302	9.9992(−1)	8.387(−11)	1.726(−2)
$3\,S_0$	2.0612721521	1	4.424(−10)	1.097(−3)	$8\,D_2$	2.0078179505	8.1157(−5)	1.008(−10)	9.959(−1)
$3\,P_1$	2.0551451572	1.0000	1.402(−8)	2.306(−2)	$8\,F_3$	2.0078133037	7.6422(−1)	4.348(−11)	2.322(−1)
$3\,P_1$	2.0580833984	6.5434(−8)	2.551(−10)	1.000	$8\,F_3$	2.0078133189	2.3578(−1)	4.351(−11)	7.746(−1)
$3\,D_2$	2.0556208958	9.9976(−1)	1.541(−9)	1.377(−3)	$8\,G_4$	2.0078127146	5.1998(−1)	2.573(−11)	3.327(−1)
$3\,D_2$	2.0556364715	2.4366(−4)	1.711(−9)	9.998(−1)	$8\,G_4$	2.0078127224	4.8002(−1)	2.573(−11)	6.970(−1)
$4\,S_0$	2.0335868114	1	2.748(−10)	9.973(−3)	$8\,H_5$	2.0078125740	5.1525(−1)	1.699(−11)	3.686(−1)
$4\,P_1$	2.0310691570	1.0000	6.100(−9)	2.757(−2)	$8\,H_5$	2.0078125792	4.8475(−1)	1.699(−11)	6.805(−1)
$4\,P_1$	2.0323253374	6.2400(−8)	1.746(−10)	1.000	$8\,I_6$	2.0078125300	5.1289(−1)	1.205(−11)	3.886(−1)
$4\,D_2$	2.0312799444	9.9987(−1)	6.524(−10)	7.043(−3)	$8\,I_6$	2.0078125337	4.8711(−1)	1.205(−11)	6.737(−1)
$4\,D_2$	2.0312889381	1.2987(−4)	7.545(−10)	9.999(−1)	$8\,K_7$	2.0078125134	5.1117(−1)	9.013(−12)	4.015(−1)
$4\,F_3$	2.0312551467	6.3506(−1)	3.345(−10)	3.518(−1)	$8\,K_7$	2.0078125162	4.8883(−1)	9.012(−12)	6.705(−1)
$4\,F_3$	2.0312552539	3.6494(−1)	3.346(−10)	6.496(−1)	$9\,S_0$	2.0063695649	1	3.420(−11)	1.750(−2)
$5\,S_0$	2.0211769075	1	1.650(−10)	1.352(−2)	$9\,P_1$	2.0061563442	1.0000	5.555(−10)	3.046(−2)
$5\,P_1$	2.0199057427	1.0000	3.171(−9)	2.904(−2)	$9\,P_1$	2.0062673547	5.9731(−8)	2.454(−11)	9.997(−1)
$5\,P_1$	2.0205516925	6.1157(−8)	1.103(−10)	1.000	$9\,D_2$	2.0061756842	9.9992(−1)	5.917(−11)	1.833(−2)
$5\,D_2$	2.0200158953	9.9990(−1)	3.368(−10)	1.111(−2)	$9\,D_2$	2.0061766964	7.8814(−5)	7.131(−11)	9.953(−1)
$5\,D_2$	2.0200210810	1.0230(−4)	3.969(−10)	9.986(−1)	$9\,F_3$	2.0061734120	7.7270(−1)	3.074(−11)	2.248(−1)
$5\,F_3$	2.0200029491	6.9758(−1)	1.730(−10)	2.929(−1)	$9\,F_3$	2.0061734228	2.2730(−1)	3.077(−11)	7.824(−1)
$5\,F_3$	2.0200030066	3.0242(−1)	1.731(−10)	7.108(−1)	$9\,G_4$	2.0061729942	5.2014(−1)	1.820(−11)	3.279(−1)
$5\,G_4$	2.0200007114	5.1909(−1)	1.030(−10)	3.742(−1)	$9\,G_4$	2.0061729997	4.7986(−1)	1.820(−11)	7.019(−1)
$5\,G_4$	2.0200007432	4.8091(−1)	1.030(−10)	6.559(−1)	$9\,H_5$	2.0061728939	5.1525(−1)	1.201(−11)	3.641(−1)
$6\,S_0$	2.0145631337	1	1.038(−10)	1.532(−2)	$9\,H_5$	2.0061728975	4.8475(−1)	1.201(−11)	6.851(−1)
$6\,P_1$	2.0138338389	1.0000	1.852(−9)	2.971(−2)	$9\,I_6$	2.0061728622	5.1289(−1)	8.512(−12)	6.772(−1)
$6\,P_1$	2.0142082520	6.0516(−8)	7.148(−11)	9.999(−1)	$9\,I_6$	2.0061728648	4.8711(−1)	8.511(−12)	3.851(−1)
$6\,D_2$	2.0138982650	9.9991(−1)	1.964(−10)	1.389(−2)	$9\,K_7$	2.0061728501	5.1117(−1)	6.349(−12)	3.974(−1)
$6\,D_2$	2.0139014493	9.0800(−5)	2.339(−10)	9.975(−1)	$9\,K_7$	2.0061728520	4.8883(−1)	6.349(−12)	6.745(−1)
$6\,F_3$	2.0138906946	7.3160(−1)	1.012(−10)	2.614(−1)	$9\,L_8$	2.0061728451[a]	5.0985(−1)	4.926(−12)	4.061(−1)
$6\,F_3$	2.0138907291	2.6840(−1)	1.013(−10)	7.437(−1)	$9\,L_8$	2.0061728462[a]	4.9015(−1)	4.926(−12)	6.731(−1)
$6\,G_4$	2.0138893488	5.1947(−1)	6.000(−11)	3.524(−1)	$10\,S_0$	2.0051430006	1	2.534(−11)	1.783(−2)
$6\,G_4$	2.0138893672	4.8053(−1)	6.000(−11)	6.775(−1)	$10\,P_1$	2.0049879545	1.0000	4.058(−10)	3.056(−2)
$6\,H_5$	2.0138890361	5.1525(−1)	3.980(−11)	3.864(−1)	$10\,P_1$	2.0050688692	5.9634(−8)	1.831(−11)	9.997(−1)
$6\,H_5$	2.0138890484	4.8475(−1)	3.980(−11)	6.629(−1)	$10\,D_2$	2.0050020812	9.9992(−1)	4.329(−11)	1.915(−2)
$7\,S_0$	2.0106257997	1	6.877(−11)	1.637(−2)	$10\,D_2$	2.0050028267	7.7197(−5)	5.226(−11)	9.949(−1)
$7\,P_1$	2.0101692270	1.0000	1.173(−9)	3.008(−2)	$10\,F_3$	2.0050004215	7.7867(−1)	2.254(−11)	2.198(−1)
$7\,P_1$	2.0104051450	6.0123(−8)	4.824(−11)	9.998(−1)	$10\,F_3$	2.0050004295	2.2133(−1)	2.256(−11)	7.878(−1)
$7\,D_2$	2.0102100536	9.9992(−1)	1.245(−10)	1.584(−2)	$10\,G_4$	2.0050001149	5.2026(−1)	1.336(−11)	3.246(−1)
$7\,D_2$	2.0102121286	8.4763(−5)	1.491(−10)	9.966(−1)	$10\,G_4$	2.0050001188	4.7974(−1)	1.336(−11)	7.052(−1)
$7\,F_3$	2.0102052566	7.5158(−1)	6.437(−11)	2.433(−1)	$10\,H_5$	2.0050000409	5.1526(−1)	8.814(−12)	3.609(−1)
$7\,F_3$	2.0102052789	2.4842(−1)	6.442(−11)	7.627(−1)	$10\,H_5$	2.0050000435	4.8474(−1)	8.814(−12)	6.883(−1)
$7\,G_4$	2.0102043898	5.1977(−1)	3.810(−11)	3.402(−1)	$10\,I_6$	2.0050000174	5.1289(−1)	6.241(−12)	6.801(−1)
$7\,G_4$	2.0102044014	4.8023(−1)	3.810(−11)	6.896(−1)	$10\,I_6$	2.0050000193	4.8711(−1)	6.241(−12)	3.823(−1)
$7\,H_5$	2.0102041850	5.1525(−1)	2.519(−11)	3.755(−1)	$10\,K_7$	2.0050000083	5.1117(−1)	4.649(−12)	3.950(−1)
$7\,H_5$	2.0102041928	4.8475(−1)	2.519(−11)	6.737(−1)	$10\,K_7$	2.0050000098	4.8883(−1)	4.649(−12)	6.769(−1)
$7\,I_6$	2.0102041217	5.1289(−1)	1.792(−11)	6.671(−1)	$10\,L_8$	2.0050000046[a]	5.0985(−1)	3.600(−12)	4.035(−1)
$7\,I_6$	2.0102041273	4.8711(−1)	1.792(−11)	3.953(−1)	$10\,L_8$	2.0050000054[a]	4.9015(−1)	3.600(−12)	6.757(−1)
$8\,S_0$	2.0080936385	1	4.761(−11)	1.704(−2)	$10\,M_9$	2.0050000028[a]	5.0881(−1)	2.874(−12)	4.097(−1)
$8\,P_1$	2.0077890691	1.0000	7.887(−10)	3.031(−2)	$10\,M_9$	2.0050000032[a]	4.9119(−1)	2.874(−12)	6.752(−1)

[a]Extrapolated.

[43,49]. It can be shown that the fluorescence decay branching ratio $\Gamma_{k,b}^f/(\Gamma_b^f+\Gamma_b^a)$ is additionally enhanced by a factor $(1+1/q_{kb}^2)$ due to the coupling to the continuum, where q_{kb} is the asymmetry parameter associated with the $|b\rangle \rightarrow |k\rangle$ transition [50,51]. The branching ratios ($\mathcal{B}_b^m$) are modified accordingly. However, the effect of the correction factors on the decay branching ratios has been found to be negligible in the present case.

The single-photon shifts and widths have been assessed from the real and imaginary parts of

$$\frac{S_g - i\gamma_g/2}{\mathcal{F}^2} = \frac{1}{4}\sum_{\nu}\frac{\langle g_\theta^*|D_\theta^\dagger|\nu_\theta\rangle\langle\nu_\theta^*|D_\theta|g_\theta\rangle}{\epsilon_g + \omega_0 - E_\nu^\theta}, \tag{26a}$$

$$\frac{S_b - i\gamma_b/2}{\mathcal{F}^2} \approx \frac{1}{4}\sum_{\mu}\left\{\frac{\langle b_\theta^*|D_\theta^\dagger|\mu_\theta\rangle\langle\mu_\theta^*|D_\theta|b_\theta\rangle}{\tilde{\epsilon}_b + \omega_0 - E_\mu^\theta} + \frac{\langle b_\theta^*|D_\theta|\mu_\theta\rangle\langle\mu_\theta^*|D_\theta^\dagger|b_\theta\rangle}{\tilde{\epsilon}_b - \omega_0 - E_\mu^\theta}\right\}. \tag{26b}$$

The resonance states we consider are slowly decaying, so that their autoionization widths are small. The contribution to the imaginary part on the right-hand side of Eq. (26b) due to the complex nature of the wave function corresponding to $|b_\theta\rangle$ [44,52] is therefore small compared to the contribution of states $|\mu_\theta\rangle$ which represent the continuum. It is thus a good approximation to treat the resonance state as stable, as has been done in Eq. (26b). The contribution of the second term in Eq. (26b) to the total rate was found to be negligible compared to the contribution of the first term. Note that the leading configurations of the $^1S^e$ and $^1D^e$ autoionizing states below $N = 2$ are $2s n\ell$ and $2p n\ell'$ ($\ell = s,d$; $\ell' = p,f$). These are coupled to the $1s\epsilon\ell$ continuum configurations. The dominant contribution to the dipole transition amplitude connecting the resonance state to the $1s\epsilon p$ continuum is therefore due to the (weak) $1s\epsilon\ell - 1s\epsilon p$ coupling. Contrary to γ_b, the second term must be included in the calculation of the field-induced shift (S_b), as has already been mentioned.

The single-photon ionization rates pertaining to $|g\rangle$ and $|b\rangle$ can be calculated from the respective ionization cross sections, σ_g and σ_b, using $\gamma_j = \sigma_j\mathcal{F}^2/(8\pi\alpha\omega_0)$, where $j = g,b$. We have taken into account that the intensity of the pulse, which we denote by $I(t)$, and the electric-field amplitude are related through

$$I(t) = \mathcal{F}^2(t)/(8\pi\alpha), \tag{27}$$

where $I(t)$ is given in units of $E_H^2/(a_0^2\hbar) \approx 6.44 \times 10^{15}$ W/cm^2 (E_H is the Hartree energy and a_0 the Bohr radius). Since the ground-state ionization cross section does not vary strongly with ω_0 in the energy region of the resonances, its value has been kept fixed to the cross section near the $2\,(1,0)^+\ ^1S^e$ resonance for simplicity: $\sigma_g = 0.20$ a.u. $\approx 5.6 \times 10^{-18}$ cm^2.

The second-order ground-state ionization rate $\Re_g$ from Eq. (18b) has been calculated from the generalized two-photon background ionization cross sections given in Ref. [40]. The total two-photon cross section is written as $\bar{\sigma}_g = \bar{\sigma}_g(1s\epsilon s) + \bar{\sigma}_g(1s\epsilon d)$, where the two terms describe transitions to the $^1S^e$ and $^1D^e$ continuum. The connection between the two-photon ionization rate and the cross section is $\Re_g = \bar{\sigma}_g\mathcal{F}^4/(8\pi\alpha\omega_0)^2$. As for the single-photon ionization cross section, the energy dependence of the total background two-photon cross section has been disregarded. The value used in the calculations is $\bar{\sigma}_g(1s\epsilon s) + \bar{\sigma}_g(1s\epsilon d) = 0.011$ a.u. $\approx 2.18 \times 10^{-52}$ cm^{4}s, which corresponds to the total cross section near the $2\,(1,0)^+ {}^1S^e$ resonance. Except for two-photon rate $\Re_g$, which is needed to describe nonresonant two-photon ionization, the two-photon shift and width have not been included in the present calculations since they are much smaller than their single-photon analogs.

The asymmetry parameters have been taken from Ref. [40]. Since, for $J_g = M_g = 0$, the only possible value of the total angular momentum of the intermediate states is $J_\nu = 1$, the asymmetry parameters of the resonance states can be shown to be independent of M_b.

The resonance parameters used in the calculation are given in Table II. The incident light was taken to be linearly polarized, with the quantization (z) axis chosen parallel to $\hat{\boldsymbol{\epsilon}}_0$. Since the basis states are real, $\tilde{\Omega}_{bg} = \tilde{\Omega}_{gb}$. The net field-induced shift has been denoted by $S_{bg} = S_b - S_g$. The states have been labeled by $n\,(K,T)^A$, where n is the principal quantum number of the "outer" electron and K, T, and A are the correlation quantum numbers. The details about the classification of the DES are beyond the scope of this work, and we refer the interested reader to the review of Rost *et al.* [52]. Except for the lowest-lying $^1S^e$ resonance, the Rabi frequencies and the fluorescence widths calculated using the velocity and length forms of the dipole operator are seen to agree well. The matrix elements corresponding to the two forms are related through

$$\langle b_\theta^*|e^{i\theta}D|a_\theta\rangle = \frac{\langle b_\theta^*|e^{-i\theta}\hat{\boldsymbol{\epsilon}}_0\cdot(\nabla_1 + \nabla_2)|a_\theta\rangle}{E_a^\theta - E_b^\theta}, \tag{28}$$

which follows from $\boldsymbol{p}_j e^{-i\theta} = i[H(\theta),\boldsymbol{r}_j e^{i\theta}]$, $j = 1,2$. Laser-induced shifts S_{bg} are of the same order of magnitude as the ponderomotive shift,

$$U_p(t) = 2\pi\alpha\frac{I(t)}{\omega_0^2} = \frac{\mathcal{F}^2(t)}{4\omega_0^2}. \tag{29}$$

For example, the ratio $U_p/\mathcal{F}^2$ is approximately 0.192 a.u. for the $2\,(-1,0)^+\ ^1S^e$ resonance and 0.187 a.u. for the $3\,(1,0)^+\ ^1D^e$ resonance, which is comparable to the calculated shifts found in Table II. The method used here for the calculation of the ground- and resonance state shifts gives results which agree with the values of the static [53] and dynamic [54] polarizabilities of He.

Since, for the resonances considered, $|1 - i/q_{bg}| \approx 1$, it is possible to assess the magnitudes of the two-photon Rabi frequencies from Eqs. (10) and (14a) by using the expression for the partial two-photon background ionization rate given by $\pi|\bar{\Omega}_{c_1 g}|^2/2 \equiv \bar{\sigma}_g'\mathcal{F}^4/(8\pi\alpha\omega_0)^2$:

$$\frac{|q_{bg}|\sqrt{\bar{\sigma}_g'\Gamma_b^a}}{8\pi\alpha\omega_0} = \frac{|\tilde{\Omega}_{bg}|}{\mathcal{F}^2} \approx \frac{|\tilde{\Omega}_{bg}(1 - i/q_{bg})|}{\mathcal{F}^2}. \tag{30}$$

The magnitudes obtained from the left-hand side of Eq. (30) using the values of the partial ionization cross section ($\bar{\sigma}_g'$) reported in Ref. [40] agree with the results found in Table II.

IV. RESULTS AND DISCUSSION

A. Metastable atom yield for a focused laser beam

We consider linearly polarized incident light described by time-dependent electric field

$$\boldsymbol{F}(t) = \mathcal{F}(t)\,\mathrm{Re}\{\hat{\boldsymbol{\epsilon}}_0 e^{-i\omega_0 t}\}, \tag{31}$$

with Gaussian envelope $\mathcal{F}(t) = \mathcal{F}_0\exp(-2\ln 2\,t^2/\tau^2)$, where τ is the pulse duration (the full width at half maximum, corresponding to the intensity profile) and the peak intensity is

TABLE II. Parameters of the $^1S^e$ and $^1D^e$ resonances below the $N = 2$ ionization threshold. The numbers in parentheses denote the powers of ten. For each resonance state, the parameters in the first and the second line are calculated using the velocity form and the length form of the dipole operator, respectively. The quantities which depend on ω_0 have been evaluated at the photon energy equal to $(\tilde{\epsilon}_b - \epsilon_g)/2$.

	$n\,(K,T)^A$	$-\tilde{\epsilon}_b$	Γ_b^a	Γ_b^f	$\tilde{\Omega}_{bg}(1 - i/q_{bg})/\mathcal{F}^2$	$S_{bg}/\mathcal{F}^2$	σ_b	$\mathcal{B}_b^m$	Re q_{bg}[aa]	Im q_{bg}[a]
$^1S^e$	$2\,(1,0)^+$	0.777866	4.543(−3)	6.510(−8)	1.769(−1) − *i* 7.870(−2)	0.226	3.15(−2)	5.478(−8)	−6.97	4.03
				6.509(−8)	1.738(−1) − *i* 8.519(−2)	0.303		5.476(−8)		
	$2\,(-1,0)^+$	0.621876	2.137(−4)	2.010(−7)	1.234(−1) − *i* 6.057(−2)	0.174	1.27(−2)	1.624(−6)	−20.1	−12.3
				2.010(−7)	1.240(−1) − *i* 6.080(−2)	0.174		1.624(−6)		
	$3\,(1,0)^+$	0.589893	1.363(−3)	7.553(−8)	8.017(−2) − *i* 3.143(−2)	0.116	1.65(−2)	1.108(−6)	−6.45	−4.59
				7.554(−8)	8.170(−2) − *i* 3.154(−2)	0.120		1.107(−6)		
	$3\,(-1,0)^+$	0.548080	7.469(−5)	1.385(−7)	5.567(−2) − *i* 2.217(−2)	0.112	1.29(−2)	4.269(−5)	−10.9	−4.81
				1.385(−7)	5.593(−2) − *i* 2.205(−2)	0.112		4.269(−5)		
	$4\,(1,0)^+$	0.544881	4.920(−4)	1.061(−7)	4.385(−2) − *i* 1.859(−2)	0.0987	1.35(−2)	5.486(−6)	−5.44	−8.53
				1.061(−7)	4.453(−2) − *i* 1.835(−2)	0.101		5.485(−6)		
	$4\,(-1,0)^+$	0.527714	4.624(−5)	1.120(−7)	3.935(−2) − *i* 1.456(−2)	0.0958	1.32(−2)	6.642(−5)	−8.37	−3.53
				1.120(−7)	3.952(−2) − *i* 1.444(−2)	0.0960		6.642(−5)		
$^1D^e$	$2\,(1,0)^+$	0.701907	2.363(−3)	2.656(−7)	3.123(−1) − *i* 1.819(−1)	0.366	1.64(−2)	3.586(−7)	−15.4	7.40
				2.656(−7)	3.116(−1) − *i* 1.820(−1)	0.365		3.587(−7)		
	$3\,(1,0)^+$	0.569211	5.557(−4)	1.712(−7)	1.393(−1) − *i* 7.481(−2)	0.191	1.22(−2)	8.530(−6)	−15.5	5.48
				1.713(−7)	1.392(−1) − *i* 7.509(−2)	0.191		8.530(−6)		
	$3\,(0,1)^0$	0.556425	1.990(−5)	9.599(−8)	3.078(−2) − *i* 8.850(−3)	0.116	1.42(−2)	4.350(−4)	−25.6	6.35
				9.599(−8)	3.077(−2) − *i* 8.898(−3)	0.116		4.350(−4)		
	$4\,(1,0)^+$	0.536722	2.319(−4)	1.547(−7)	8.868(−2) − *i* 4.726(−2)	0.153	1.19(−2)	2.841(−5)	−16.1	5.48
				1.547(−7)	8.867(−2) − *i* 4.743(−2)	0.153		2.841(−5)		
	$4\,(0,1)^0$	0.531510	1.109(−5)	1.098(−7)	2.277(−2) − *i* 6.386(−3)	0.122	1.33(−2)	8.885(−4)	−27.7	6.18
				1.098(−7)	2.277(−2) − *i* 6.420(−3)	0.122		8.885(−4)		
	$4\,(-1,0)^0$	0.529293	9.679(−9)	2.158(−7)	9.682(−4) − *i* 5.566(−5)	0.150	8.79(−3)	4.376(−1)	−26.2	4.05
				2.158(−7)	9.689(−4) − *i* 5.628(−5)	0.150		4.376(−1)		

[a]From Ref. [40].

given by $I_0 = \mathcal{F}_0^2/(8\pi\alpha)$. Further, we assume that the spatial profile of the incident beam is Gaussian. If we denote the coordinate along the beam axis by ζ and the coordinate perpendicular to the beam axis by ρ, the intensity near the focus ($\zeta = 0$) is described by [55,56]

$$I_0(\rho,\zeta) = \frac{I_f}{w^2(\zeta)} \exp\left(-\frac{4\ln 2\,\rho^2}{\rho_0^2 w^2(\zeta)}\right), \tag{32}$$

where $w(\zeta) = \sqrt{1 + (\zeta/\zeta_0)^2}$, I_f denotes the intensity at the focus, and ρ_0 is the focal radius. We calculate the volume-integrated yield from single-atom yields y_j ($j = m,e,f$) as

$$Y_j = 2\pi\mathcal{N} \lim_{t\to\infty} \int_{-\zeta_1}^{\zeta_1} d\zeta \int_0^{\rho_1} d\rho\, \rho\, y_j(t; I_0(\rho,\zeta)), \tag{33}$$

where $2\zeta_1$ and ρ_1 are the length and the radius of the cylindrically shaped interaction volume, and $\mathcal{N}$ is the density of atoms in the volume (assumed to be independent of ρ and ζ). In the calculations, we assume that $2\rho_0 = 25$ μm, $\zeta_0 = 18.75$ mm, and $\zeta_1 = 2.5$ mm, yielding the beam divergence $\rho_0/\zeta_0 \approx 1.33 \times 10^{-3}$. The density of atoms is taken to be $\mathcal{N} = 3 \times 10^{13}$ atoms/cm^3. The pulse duration and the transverse rate have been fixed to $\tau = 70$ fs ≈ 2894 a.u. and $\gamma_L = 9.5$ meV $\approx 3.5 \times 10^{-4}$ a.u. These parameters approximately match the experimental conditions of Ref. [10].

Metastable atom yield y_m, electron yield y_e, and fluorescence yield y_f calculated for peak intensity I_0 equal to 10^{12}, 10^{13}, and 10^{14} W/cm^2 in the region of the autoionizing states are shown in Fig. 2. As can be seen, isolated peaks are clearly visible in all the yields. The relative peak amplitudes remain largely unaffected by the peak intensity for $I_0 \lesssim 10^{14}$ W/cm^2. In this intensity range, the volume-integrated yields for the Gaussian spatial profile (plotted with dashed black lines) coincide—up to an overall factor—with the single-atom yields: at these intensities, the amplitude ratios of the peaks have been found to be roughly independent of the spatial profile of the pulse.

Conversely, the peak ratios in the single-atom yield change substantially when the intensity of the pulse is increased to 10^{15} W/cm^2. As shown in Fig. 3, the peaks lying at higher energies are strongly suppressed. This occurs both due to high ionization rate γ_b, which becomes comparable to or greater than the spontaneous decay rate, and due to the strong ground-state ionization. For $I_0 \gtrsim 5 \times 10^{14}$ W/cm^2, the single-atom yield is no longer approximately proportional to the volume-integrated yield, as can be seen in Fig. 3. Note, however, that the peak ratios for the Gaussian profile remain approximately the same even for high I_f: the spatial regions further away from the focus, where the intensity is lower, contribute substantially in this case.

The saturation due to the depletion of the ground-state population may be examined by studying the dependence of the peak positions and their strengths (areas under the peaks) in the MS atom yield. In this case, it is instructive to compare the results for the Gaussian spatial profile to the yield obtained using a flat-top profile:

$$\bar{Y}_m = 2\pi\rho_2^2\zeta_1\mathcal{N} \lim_{t\to\infty} y_m(t; I_f), \tag{34}$$

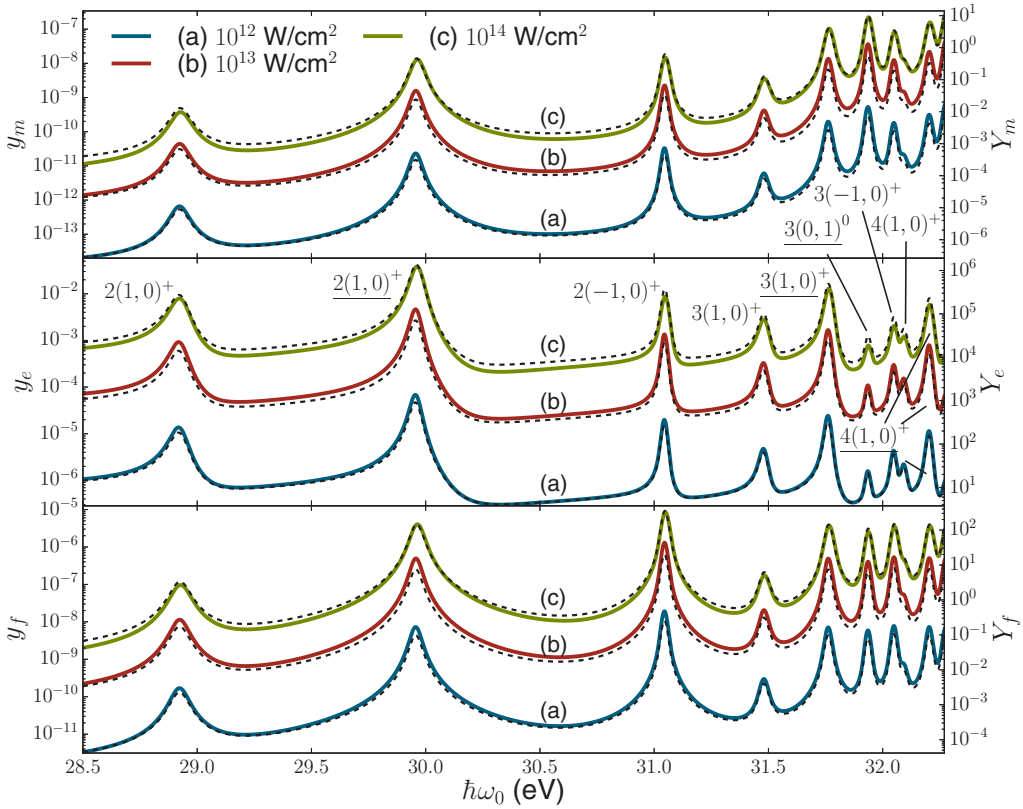

FIG. 2. (Color online) Metastable atom yield y_m (top), electron yield y_e (middle), and fluorescence yield y_f (bottom) for peak intensity I_0 equal to 10^{12}, 10^{13}, and 10^{14} W/cm^2. Dashed black lines correspond to the volume-integrated yields (Y_m, Y_e, and Y_f), as given by Eq. (33) for the intensity at the focus (I_f) set to 10^{12}, 10^{13}, and 10^{14} W/cm^2. The $^1S^e$ and $^1D^e$ (underlined) autoionizing states are labeled by correlation quantum numbers $n\,(K,T)^A$ (see Table II).

where $\rho_2 = \rho_0/\sqrt{4\,\ln 2}$ denotes the effective radius chosen to give the same total power ($\pi\rho_2^2 I_f$) as the Gaussian spatial profile. Figure 4 shows the dependence of the peak positions and the areas under the peaks for the lowest three resonance states. As can be seen, the areas start deviating from the quadratic trend at the peak intensity of roughly 2×10^{13} W/cm^2 in the case of the Gaussian pulse and slightly lower in the case of the flat-top pulse. As is well known, this saturation occurs at intensities at which the depletion of the ground-state population becomes substantial [57]. The order of magnitude is consistent with the saturation intensity (I_s) calculated from $\sigma_g I_s \tau/(\hbar\omega_0) \sim 1$.

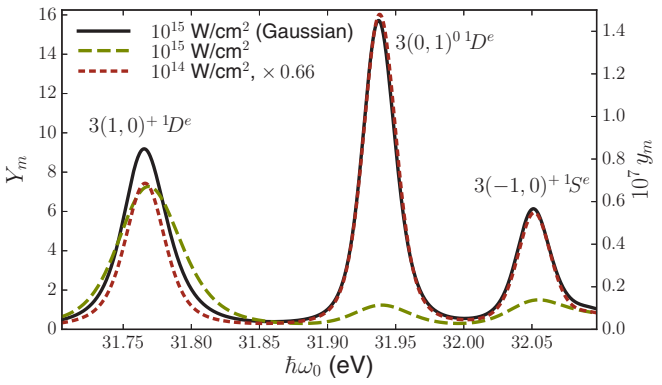

FIG. 3. (Color online) Single-atom metastable atom yield (y_m) for the peak intensity of 10^{14} W/cm^2 (fine dashed red) and 10^{15} W/cm^2 (dashed green). The volume-integrated yield (Y_m) for the Gaussian spatial profile of peak intensity 10^{15} W/cm^2 is plotted with a solid black line.

In the intensity region where no saturation occurs, we may express the effective ionization rate as $R_e = y_e/\tau_{\rm eff}$, where the effective pulse duration is

$$\tau_{\rm eff} = \int_{-\infty}^{\infty}\left(\frac{\mathcal{F}(t)}{\mathcal{F}_0}\right)^4 dt = \tau\sqrt{\frac{\pi}{8\,\ln 2}} \approx 0.75\tau. \qquad (35)$$

The order of magnitude of the effective rate for $I_0 = 10^{12}$ W/cm^2 in the region of the $2\,(1,0)^+$ $^1S^e$ and $^1D^e$ states agrees well with the rate calculated in Ref. [40].

Žitnik *et al.* [10] used the calculated dependence of the shifts and the energy-integrated MS atom yield to show that the maximum intensity of the pulses was of the order of 10^{14} W/cm^2. The measured energy shifts were seen to be of the same order of magnitude as the ponderomotive shift, as has also been demonstrated here. Furthermore, the measured saturation trend suggested that the spatial profile of the beam was closer to a profile with a cutoff radius than to a Gaussian profile.

B. Effects of higher harmonics

Photon energies of the third and higher harmonics lie above the double ionization threshold of helium. These harmonics

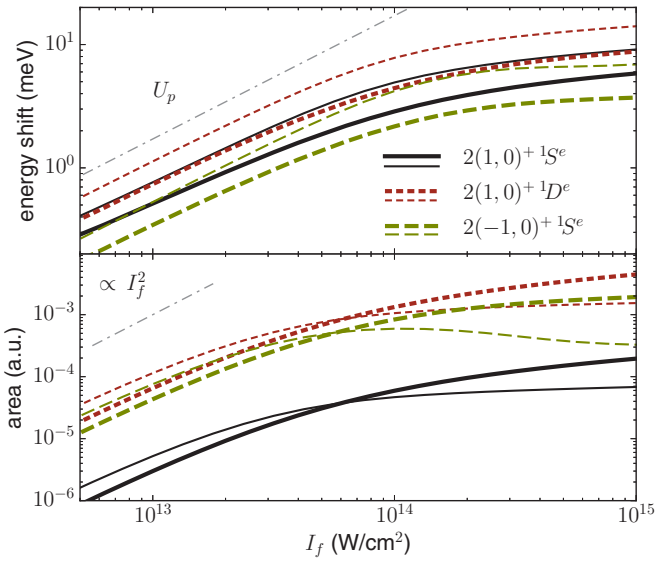

FIG. 4. (Color online) Top: the dependence of the peak positions of the lowest resonance states in the metastable atom yield (Y_m) on the intensity at the focus (I_f) for the Gaussian spatial profile (thick lines). The yield for the flat-top spatial profile ($\bar{Y}_m$, thin lines) is also shown for comparison. The ponderomotive shift (U_p) at peak intensity I_f at the energy of the $2\,(1,0)^+{}^1S^e$ resonance is plotted with a dash-dotted line. Bottom: the area under the peaks for the Gaussian and flat-top profiles. The quadratic dependence ($\propto I_f^2$) is shown to guide the eye.

result in an increase of ionization rates γ_b and γ_g. Apart from affecting the widths of the peaks and further depleting the ground-state population, they produce no additional effect in the MS atom yield. Conversely, even a relatively small admixture of the second harmonic ($\omega_1 = 2\omega_0$) can substantially modify the measured MS atom yield through single-photon excitation to one of the ${}^1P^o$ resonance states when ω_1 lies close to the resonance energy.

Let $|p\rangle$ be a discrete ${}^1P^o$ state embedded in the $1s\epsilon p$ continuum. We may take its effect into account by adding $-\gamma_g^p a_g/2 - i\tilde{\Omega}_p(1 - i/q_p)/2$ to the right-hand side of Eq. (6a) and by extending the set of equations with

$$\frac{d}{dt}a_p = i\,\Delta_p a_p - \frac{\Gamma_p}{2}a_p - i\frac{\tilde{\Omega}_p}{2}\left(1 - \frac{i}{q_p}\right)a_g, \qquad (36)$$

where a_p denotes the slowly varying amplitude corresponding to state $|p\rangle$. The single-photon ground-state ionization rate for photons with energy ω_1 analogous to γ_g is denoted by γ_g^p, $\Delta_p = \omega_1 - \epsilon_p + \epsilon_g - S_{pg} - F_p$ denotes the detuning (includes the field-induced shifts and the shift due to the CI), and Γ_p the total decay rate of state $|p\rangle$ (includes autoionization rate Γ_p^a and fluorescence rate Γ_p^f, as well as the total ionization rate). The Rabi frequency connecting the ground state to the CI-modified discrete state and the corresponding asymmetry parameter have been denoted by $\tilde{\Omega}_p$ and q_p, respectively.

The singlet MS state can be reached directly from the ${}^1P^o$ states; thus the order of magnitude of the branching ratios for the lowest few ${}^1P^o$ states is given by $\mathcal{B}_p^m \sim \Gamma_{m,p}^f/(\Gamma_p^f + \Gamma_p^a)$. The branching ratios of the $2\,(0,1)^+$, $3\,(1,0)^-$, $3\,(0,1)^+$, and $3\,(-1,0)^0 {}^1P^o$ states are 1.13×10^{-4}, 1.72×10^{-2}, 2.89×10^{-6}, and 6.38×10^{-2}, respectively. The other relevant parameters (the dipole matrix elements, asymmetry parameters, and fluorescence widths) can be found in Refs. [49,52].

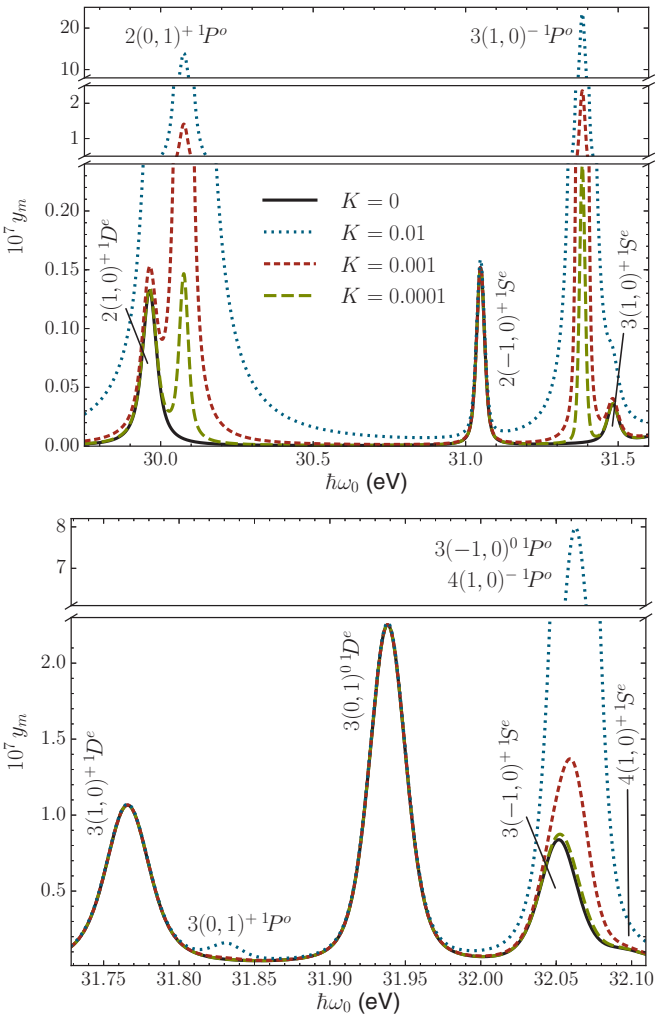

FIG. 5. (Color online) Metastable atom yield for peak intensity $I_0 = 10^{14}$ W/cm^2 and for flux ratio $K = \Phi_1/\Phi$ set to 10^{-2}, 10^{-3}, and 10^{-4}.

Figure 5 shows how the MS atom yield changes with the flux ratio defined as

$$K = \frac{\Phi_1(t)}{\Phi(t)} = \frac{I_1(t)}{I(t)}\frac{\omega_0}{\omega_1}, \qquad (37)$$

where Φ and I denote the photon flux and the intensity of the fundamental, and Φ_1 and I_1 are the flux and intensity of the second harmonic in the incident beam. The MS atom yield has been calculated by solving the extended set of the density matrix equations for $I_0 = 10^{14}$ W/cm^2. The same temporal dependence of the fundamental and the second harmonic has been assumed for simplicity.

As can be seen, an admixture as low as $K \sim 10^{-4}$ produces measurable changes in the MS atom yield in the energy region of the $2\,(0,1)^+$ and $3\,(1,0)^-$ ${}^1P^o$ resonances. For higher values of the ratio ($K \sim 10^{-2}$), photoexcitation by the second harmonic already represents the dominant process in

this energy region and in the region of the $3\,(-1,0)^0$ and $4\,(1,0)^-\ {}^1P^o$ states. Here, the MS atom yield is thus very sensitive to the admixture of the second harmonic and can be used to assess its content in the incident beam. The energy region of the $3\,(1,0)^+$ and $3\,(0,1)^0\,{}^1D^e$ states, on the other hand, is only weakly affected by the admixture: the signal due to the $3\,(0,1)^+\ {}^1P^o$ resonance remains low even for high values of parameter K. Consequently, this energy region and the region of the $2\,(-1,0)^+\ {}^1S^e$ resonance, which is also only weakly affected by the second harmonic, were used in Ref. [10] to study two-photon above-threshold excitation. In this energy region, the upper bound of parameter K was determined to be of the order of 10^{-3} based on the absence of statistically significant signal of the $^1P^o$ resonances in the MS atom yield.

C. Polarization and chirp effects

One of the unique properties of FERMI is that it can produce light pulses with variable polarization [9]. The effect of polarization of the incident light on the MS atom yield is studied most conveniently if $\hat{\boldsymbol{e}}_0$ is parametrized as

$$\hat{\boldsymbol{e}}_0 = (\hat{\boldsymbol{x}} + i\kappa\,\hat{\boldsymbol{y}})/\sqrt{1+\kappa^2}, \tag{38}$$

where $-1 \leqslant \kappa \leqslant 1$ and where it has been assumed that the beam propagates along the z axis. For $\kappa = 0$, Eq. (38) describes linearly polarized light, whereas $\kappa = 1$ and $\kappa = -1$ for right- and left-hand circularly polarized light, respectively. For $|\kappa| < 1$, Eq. (38) describes elliptically polarized light.

It is easy to show that the amplitudes of the $^1S^e$ and $^1D^e$ peaks in the MS atom yield scale approximately as

$$\begin{cases} (\kappa^2-1)^2/(\kappa^2+1)^2 & \text{for the } {}^1S^e \text{ states,} \\ (1+4\kappa^2+\kappa^4)/(\kappa^2+1)^2 & \text{for the } {}^1D^e \text{ states,} \end{cases} \tag{39}$$

relative to the amplitudes obtained with linearly polarized light. The latter holds when photoionization rate of the atom in the resonance state (proportional to σ_b) is weak in comparison with the total spontaneous decay rate. This has been demonstrated in Fig. 6. Note that the signal is invariant to the change of sign of κ, which is a consequence of the fact that a center of symmetry exists. Apart from its handedness, polarization of the incident light could thus, in principle, be

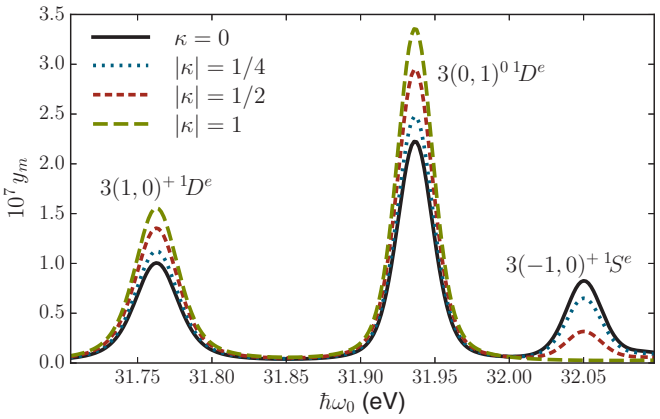

FIG. 6. (Color online) Dependence of the metastable atom yield on parameter κ. The peak intensity has been set to 10^{14} W/cm^2.

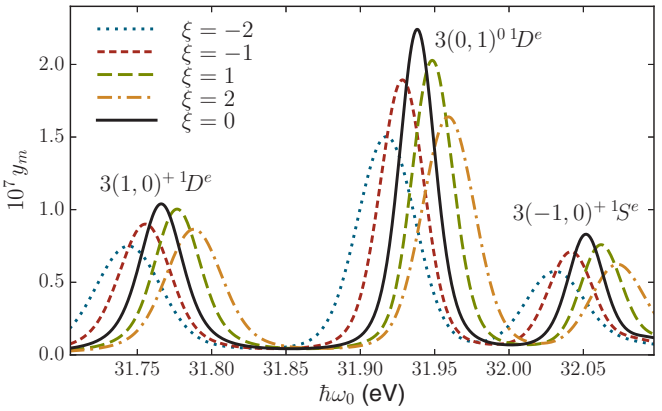

FIG. 7. (Color online) Dependence of the metastable atom yield on chirp parameter ξ.

analyzed by studying the relative peak ratios of the $^1S^e$ and $^1D^e$ states.

The present formalism can also be extended to study the effect of a (linear) pulse chirp if one replaces the harmonic factors $\exp\{\pm 2i\omega_0 t\}$ with $\exp\{\pm 2i\phi(t)\}$ in $\bar{D}$ [Eq. (1d)], where

$$\phi(t) = \omega_0 t + 2\xi\,\ln 2\frac{t^2}{\tau^2} \tag{40}$$

is the time-dependent phase of the field, and ω_0 in Eq. (9) with the instantaneous frequency given by

$$\omega_i(t) = \frac{d\phi(t)}{dt} = \omega_0 + 4\xi\,\ln 2\frac{t}{\tau^2}. \tag{41}$$

The dimensionless chirp parameter has been denoted by ξ in Eqs. (40) and (41). In Fig. 7, we show how the MS atom yield changes when the chirp parameter is varied. As can be seen, the effect of the chirp remains weak even for relatively high values of the parameter ($|\xi| \sim 2$): the peaks are only slightly shifted and broadened as the magnitude of the parameter is increased, while the intensity ratios of the peaks are only weakly affected.

V. SUMMARY

We have studied two-photon above-threshold excitation to the lowest $^1S^e$ and $^1D^e$ autoionizing states of the helium atom. Our model is based on an effective Hamiltonian operator and formulated in the framework of the density matrix. We have reported the relevant parameters used in the description of the driving by a pulsed free-electron-laser source: two-photon Rabi frequencies and laser-induced shifts and widths. The comparison of the parameters with the values obtained from the theoretical two-photon ionization cross sections and dynamic polarizabilities found in the literature indicates that the parameter values are reliably calculated. The radiative and autoionization decay of the resonance states have been taken into account. Excitation to the resonance states has been studied by examining the yield of atoms in the metastable $1s2s$ states, to which the resonance states cascade radiatively. The cascade branching ratios for both the resonance states and the $1s n\ell$ states, through which the cascade decay proceeds, represent an important ingredient of the present model. The branching ratios and other parameters may be useful for future

experiments or as benchmark results. Furthermore, we have studied the dependence of the metastable atom yield on the intensity of the beam. We have examined the influence of the second harmonic, which has been found to be strong and generally needs to be taken into account, and the effect of polarization of the incident light, which affects the $^1S^e$ versus $^1D^e$ peak ratios. Finally, we have shown that the effect of the pulse chirp on the intensity ratios is weak. The measurement of the yield of atoms in the metastable states therefore represents a relatively efficient and robust way of detecting two-photon transitions in the energy region of the autoionizing states of helium below the second ionization threshold.

ACKNOWLEDGMENTS

The authors acknowledge the financial support of the Slovenian Research Agency (research program No. P1–0112).

[1] J. Andruszkow *et al.*, Phys. Rev. Lett. **85**, 3825 (2000).
[2] W. Ackermann *et al.*, Nat. Photon. **1**, 336 (2007).
[3] P. Emma *et al.*, Nat. Photon. **4**, 641 (2010).
[4] T. Ishikawa *et al.*, Nat. Photon. **6**, 540 (2012).
[5] C. Weninger, M. Purvis, D. Ryan, R. A. London, J. D. Bozek, C. Bostedt, A. Graf, G. Brown, J. J. Rocca, and N. Rohringer, Phys. Rev. Lett. **111**, 233902 (2013).
[6] L.-H. Yu *et al.*, Science **289**, 932 (2000).
[7] G. De Ninno, E. Allaria, M. Coreno, F. Curbis, M. B. Danailov, E. Karantzoulis, A. Locatelli, O. Menteş, M. A. Nino, C. Spezzani, and M. Trovò, Phys. Rev. Lett. **101**, 053902 (2008).
[8] Z. T. Zhao *et al.*, Nat. Photon. **6**, 360 (2012).
[9] E. Allaria *et al.*, Nat. Photon. **6**, 699 (2012).
[10] M. Žitnik *et al.*, Phys. Rev. Lett. **113**, 193201 (2014).
[11] V. Lyamayev *et al.*, J. Phys. B **46**, 164007 (2013).
[12] R. P. Madden and K. Codling, Phys. Rev. Lett. **10**, 516 (1963).
[13] G. Tanner, K. Richter, and J.-M. Rost, Rev. Mod. Phys. **72**, 497 (2000).
[14] J. R. Harries, J. P. Sullivan, J. B. Sternberg, S. Obara, T. Suzuki, P. Hammond, J. Bozek, N. Berrah, M. Halka, and Y. Azuma, Phys. Rev. Lett. **90**, 133002 (2003).
[15] K. C. Prince, M. Coreno, R. Richter, M. de Simone, V. Feyer, A. Kivimäki, A. Mihelič, and M. Žitnik, Phys. Rev. Lett. **96**, 093001 (2006).
[16] C. Såthe, M. Ström, M. Agåker, J. Söderström, J.-E. Rubensson, R. Richter, M. Alagia, S. Stranges, T. W. Gorczyca, and F. Robicheaux, Phys. Rev. Lett. **96**, 043002 (2006).
[17] K. Bučar, M. Žitnik, A. Mihelič, F. Penent, P. Lablanquie, J. Palaudoux, L. Andrić, M. Braune, and R. Püttner, Phys. Rev. A **90**, 013412 (2014).
[18] M. Ström, C. Såthe, M. Agåker, J. Söderström, J.-E. Rubensson, S. Stranges, R. Richter, M. Alagia, T. W. Gorczyca, and F. Robicheaux, Phys. Rev. Lett. **97**, 253002 (2006).
[19] B. Krässig, E. P. Kanter, S. H. Southworth, R. Guillemin, O. Hemmers, D. W. Lindle, R. Wehlitz, and N. L. S. Martin, Phys. Rev. Lett. **88**, 203002 (2002).
[20] B. Krässig, E. P. Kanter, S. H. Southworth, L. Young, R. Wehlitz, B. A. deHarak, and N. L. S. Martin, Phys. Rev. A **86**, 053408 (2012).
[21] J.-E. Rubensson, C. Såthe, S. Cramm, B. Kessler, S. Stranges, R. Richter, M. Alagia, and M. Coreno, Phys. Rev. Lett. **83**, 947 (1999).
[22] M. K. Odling-Smee, E. Sokell, P. Hammond, and M. A. MacDonald, Phys. Rev. Lett. **84**, 2598 (2000).
[23] K. C. Prince, R. Richter, M. de Simone, M. Alagia, and M. Coreno, Phys. Rev. A **68**, 044701 (2003).
[24] E. Sokell, A. A. Wills, P. Hammond, M. A. MacDonald, and M. K. Odling-Smee, J. Phys. B **29**, L863 (1996).
[25] F. Penent, P. Lablanquie, R. I. Hall, M. Žitnik, K. Bučar, S. Stranges, R. Richter, M. Alagia, P. Hammond, and J. G. Lambourne, Phys. Rev. Lett. **86**, 2758 (2001).
[26] J. G. Lambourne, F. Penent, P. Lablanquie, R. I. Hall, M. Ahmad, M. Žitnik, K. Bučar, P. Hammond, S. Stranges, R. Richter, M. Alagia, and M. Coreno, J. Phys. B **36**, 4339 (2003).
[27] R. S. Van Dyck, C. E. Johnson, and H. A. Shugart, Phys. Rev. A **4**, 1327 (1971).
[28] S. S. Hodgman, R. G. Dall, L. J. Byron, K. G. H. Baldwin, S. J. Buckman, and A. G. Truscott, Phys. Rev. Lett. **103**, 053002 (2009).
[29] C. Cohen-Tannoudji, J. Dupont-Roc, and G. Grynberg, *Atom-Photon Interactions, Basic Processes and Applications* (Wiley-VCH, Weinheim, 2004).
[30] P. Lambropoulos and P. Zoller, Phys. Rev. A **24**, 379 (1981).
[31] G. Alber and P. Zoller, Phys. Rev. A **27**, 1373 (1983).
[32] T. Nakajima and P. Lambropoulos, Phys. Rev. A **50**, 595 (1994).
[33] T. Nakajima and G. Buica, Phys. Rev. A **71**, 013413 (2005).
[34] K. R. Dastidar and P. Lambropoulos, Phys. Rev. A **29**, 183 (1984).
[35] S. M. Barnett and P. M. Radmore, *Methods in Theoretical Quantum Optics* (Clarendon, Oxford, 1997).
[36] P. L. Knight, M. A. Lauder, and B. J. Dalton, Phys. Rep. **190**, 1 (1990).
[37] L. B. Madsen, P. Schlagheck, and P. Lambropoulos, Phys. Rev. A **62**, 062719 (2000).
[38] U. Fano, Phys. Rev. **124**, 1866 (1961).
[39] E. Cormier, H. Bachau, and J. Zhang, J. Phys. B **26**, 4449 (1993).
[40] I. Sánchez, H. Bachau, and E. Cormier, J. Phys. B **28**, 2367 (1995).
[41] A. T. Georges and P. Lambropoulos, Phys. Rev. A **18**, 587 (1978).
[42] G. Lagmago Kamta, B. Piraux, and A. Scrinzi, Phys. Rev. A **63**, 040502 (2001).
[43] A. Mihelič and M. Žitnik, Phys. Rev. Lett. **98**, 243002 (2007).
[44] A. Buchleitner, B. Grémaud, and D. Delande, J. Phys. B **27**, 2663 (1994).
[45] M. Žitnik, K. Bučar, M. Štuhec, F. Penent, R. I. Hall, and P. Lablanquie, Phys. Rev. A **65**, 032520 (2002).
[46] G. W. F. Drake, in *Handbook of Atomic, Molecular, and Optical Physics*, edited by G. W. F. Drake (Springer, New York, 2006).
[47] A. Mihelič, M. Žitnik, K. C. Prince, M. Coreno, and R. Richter, Phys. Rev. A **85**, 023421 (2012).

[48] A. Mihelič, M. Žitnik, K. Bučar, L. Avaldi, and R. Richter, Phys. Rev. A **89**, 063422 (2014).
[49] A. Mihelič, Ph.D. thesis, University of Ljubljana, 2006, http://www.rcp.ijs.si/amihelic/phd/thesis.pdf.
[50] L. Armstrong, C. E. Theodosiou, and M. J. Wall, Phys. Rev. A **18**, 2538 (1978).
[51] S. L. Haan and J. Cooper, Phys. Rev. A **28**, 3349 (1983).
[52] J.-M. Rost, K. Schulz, M. Domke, and G. Kaindl, J. Phys. B **30**, 4663 (1997).
[53] C. A. Nicolaides and S. I. Themelis, J. Phys. B **26**, L387 (1993).
[54] T. Mercouris, S. I. Themelis, and C. A. Nicolaides, Phys. Rev. A **61**, 013407 (1999).
[55] R. Santra and C. H. Greene, Phys. Rev. A **70**, 053401 (2004).
[56] B. E. A. Saleh and M. C. Teich, *Fundamentals of Photonics*, 2nd ed. (Wiley, Hoboken, NJ, 2007).
[57] M. G. Makris, P. Lambropoulos, and A. Mihelič, Phys. Rev. Lett. **102**, 033002 (2009).